Phase competition in trisected superconducting dome: Supporting Information

Contents

S.1. SAMPLES

TABLE I: Summary of samples shown in Fig. 2 of manuscript with their composition and experimental setup. ΓY refers to cuts taken parallel to the (0,0)-(π,π) line and ΓM refers to cuts taken parallel to (π,0)-(π,π). Dopings in manuscript determined from T_c via an empirical curve, T_c=$T_{c,max}$*[1-82.6(p-0.16)^2], taking 96K as the optimum T_c for Bi-2212 [S1].

Sample	Composition	Temperature (Fig. 2)	Experiment
UD22	Bi_2Sr_2(Ca,Dy)$Cu_2O_{8+\delta}$	10	7eV, ΓY
UD34	Bi_2Sr_2(Ca,Dy)$Cu_2O_{8+\delta}$	11	7eV, ΓY
UD40	Bi_2Sr_2(Ca,Dy/Y)$Cu_2O_{8+\delta}$	12	7eV, ΓY; 19eV, ΓY
UD50	Bi_2Sr_2(Ca,Y)$Cu_2O_{8+\delta}$	10	19eV, ΓY
UD55	Bi_2Sr_2(Ca,Dy)$Cu_2O_{8+\delta}$	11	7eV, ΓY
UD65	$Bi_{2+x}Sr_{2-x}CaCu_2O_{8+\delta}$	12	7eV, ΓY
UD75	$Bi_2Sr_2CaCu_2O_{8+\delta}$	10	22.7eV, ΓM
UD83	$Bi_2Sr_2CaCu_2O_{8+\delta}$	13	7eV, ΓY
UD85	$Bi_2Sr_2CaCu_2O_{8+\delta}$	13	22.7eV, ΓM
UD92	$Bi_2Sr_2CaCu_2O_{8+\delta}$	10	7eV, ΓY; 22.7eV, ΓM
OP96	Bi_2Sr_2(Ca,Y)$Cu_2O_{8+\delta}$	10	21.2eV, ΓY
OP98	$(Bi,Pb)_2Sr_2CaCu_2O_{8+\delta}$	30	18.4eV, ΓM
OD92	$(Bi,Pb)_2Sr_2CaCu_2O_{8+\delta}$	10	18.4eV, ΓY
OD86	$Bi_2Sr_2CaCu_2O_{8+\delta}$	18	22.7eV, ΓM
OD80	$(Bi,Pb)_2Sr_2CaCu_2O_{8+\delta}$	12,30	7eV, ΓY; 18.4eV, ΓM
OD71	$(Bi,Pb)_2Sr_2CaCu_2O_{8+\delta}$	30	18.4eV, ΓM
OD65	$(Bi,Pb)_2Sr_2CaCu_2O_{8+\delta}$	10, 18	7eV, 21.2eV, ΓY

S.2. FITTING

The energy gap in energy distribution curves (EDCs) can be quantified by several metrics: the position of the leading edge midpoint (LEM) relative to E_F, the energy positions of a quasiparticle peak, or by fitting data to an assumed model. The first two methods do not take the lineshape into account, and are less suitable for comparing gaps among samples with different dopings. Thus, we determined the gap at each cut by fitting symmetrized EDCs at the Fermi wavevector, k_F, to a minimal model proposed by Norman *et al.* [S2], $\Sigma(\mathbf{k}, \omega)$=-$i\Gamma_1 + \Delta^2/[(\omega+i0^+) + \epsilon(\mathbf{k})]$, where Γ_1 is a single particle scattering rate, $\epsilon(\mathbf{k})$ is the dispersion, and the gap, Δ, is the quantity of interest in the fitting. It is assumed that $\epsilon(\mathbf{k}_F)$=0, and k_F is defined by the minimum gap locus. A quadratic background was also included to fully account for the lineshape in the deeply underdoped regime or at momenta far from the node. This fitting is applicable to our data as long as a peak is visible in the EDC. In Fig. S1, we show the low energy portion (ω<110meV) of symmetrized EDCs at low temperature together with fits. In laser ARPES data, EDC peaks become smaller away from the node, which is not intrinsic for most dopings. Synchrotron data taken at higher photoenergy with cuts parallel to ΓM do not show such a substantial decrease in peak intensity [S3, S4], with the exception of deeply underdoped samples (p<0.09). The intensity of the quasiparticle peak relative to the higher energy part of the spectrum is also generally not intrinsic, but comparisons between different dopings can be made if experimental conditions (photoenergy, polarization, cut geometry) are identical. EDC peaks become smaller and broader with decreasing doping, a correlation and disorder effect, as widely reported [S5], and the model we use provides a good fit to all data throughout the doping range, even though it is a minimal model and does not capture the full physics of the system. In phase region **A**, the near-nodal EDCs show low-energy peaks which are narrow enough for a gap energy to be assessed accurately, though these peaks are not strictly quasiparticle-like because the width is larger than the binding energy.

Figure S2 shows gaps at all measured temperatures for a number of dopings, as a supplement to Fig. 4(d)-(e) in the manuscript. The momentum region where the gap diminishes near T_c is shaded in pink. Figure S3 shows the single particle scattering rate Γ_1 from fitting for select samples (UD40, UD65, UD92), and EDCs at a selected momentum. We note that there are momenta for UD40 and UD34 where the fitted gap increases slightly with

temperature, and this is also visible in raw EDCs, as shown in Fig. S3(d).

S.3. ANTINODAL GAPS, COMPARISON TO PREVIOUSLY PUBLISHED DATA, AND SCALING WITH T_c

Tanaka *et al.* previously reported the doping-dependence of the antinodal extrapolation of the near-nodal gap Δ_0 [S6], a quantity nominally equivalent to the near-nodal gap slope, v_Δ. A comparison between the data published by Tanaka *et al.* and data in this manuscript are shown in Fig. S4. The precision of laser ARPES allows us to draw the more definitive conclusion that near-nodal gaps are independent of doping for $0.076 \leq p \leq 0.19$. Fig. S4 also shows Δ_{AN}, the gap extracted from fitting symmetrized EDCs at the antinode. All data are $T \ll T_c$. When the gap function deviates strongly from a simple d-wave form, ($\Delta_{AN} > (v_\Delta, \Delta_0)$), Δ_0 will depend on how much of the near-nodal Fermi surface (FS) is considered in the extrapolation, which is why there is a larger difference between Δ_0 and v_Δ for $p < 0.12$.

Δ_{AN} is extracted by fitting the energy position of the superconducting quasiparticle peak at the antinode (the strongly peaked features in Fig. S4(c)), and it is plotted in Fig. S4(a). Values quantitatively agree with area-averaged STS [S7]. Δ_{AN} increases with underdoping $p < 0.12$ (pseudogap energy scale sufficiently dominates superconductivity), shows weak doping dependence for $0.12 \leq p \leq 0.19$ (superconductivity and pseudogap have similar energy scales), and decrease with increasing doping $p > 0.19$ (superconductivity over entire FS in ground state). While the energy position of the antinodal quasiparticle peak (Δ_{AN}) can be strongly influenced by the underlying pseudogap, the distinction between the two is important. This is clearly illustrated for the case of La-Bi2201 (Ref. [S8]) where the energy scales of superconductivity and the pseudogap are well separated: the antinodal superconducting feature appears as a shoulder at 30 meV, the antinodal pseudogap feature appears as a broad hump near 70 meV, and the simple d-wave extrapolation of near-nodal gaps to the antinode is 15 meV. The energy position of the superconducting shoulder feature at the antinode is not that of near-nodal superconductivity or the antinodal pseudogap, but it is affected by both–a superconducting feature whose energy position is pushed to higher binding energy near the antinode because of the underlying pseudogap. Similarly, in Bi-2212 when the gap function deviates strongly from a simple d-wave form near the antinode, the energy position

of the antinodal quasiparticle peak (Δ_{AN}) is not a measure of superconducting or pseudogap order parameters. However, Δ_{AN} does follow the doping dependence of T* in the doping regime p<0.12, indicating that it reflects strong pseudogap physics. In Fig. 4(a)-(c) of the manuscript, the dopings UD40, UD65, and UD92 are chosen to be in a doping regime where superconductivity and pseudogap energy scales are separated to varying degree. The gaps plotted in those figures are always derived from superconducting features, but the differing doping and temperature dependencies arise from varying influences of the underlying pseudogap on the energy position of the superconducting features.

As discussed in the manuscript, the precise doping where the gap function deviates from a simple *d*-wave form depends on the relative energy scales of the antinodal pseudogap and the near-nodal superconductivity. Fig. S4 indicates that there is a doping range 0.12≤p≤0.19 where Δ_{AN} is almost independent of doping and the gap function is close to a simple *d*-wave form (defined at $v_\Delta \approx \Delta_{AN}$); notably, in this doping range, T* decreases with doping (Fig. 4(f) of manuscript). This itself is a non-trivial observation which provides additional evidence that the pseudogap is suppressed by superconductivity below T_c, because the antinodal region assumes the doping-independence of near-nodal gaps, rather than the doping-dependence of T*. It must be noted that although a slight curvature away from a simple *d*-wave form is observed in laser-ARPES data for UD83 and UD92, both with p≥0.12, but $v_\Delta \approx \Delta_{AN}$ in those samples, such that near-nodal and antinodal energy scales are similar and the gap function is not considered to deviate strongly from a simple *d*-wave form. Nevertheless, this slight curvature of the gap function may be important for understanding subtleties of pseudogap/superconductivity coexistence.

For p<0.076, our new data shows somewhat similar behavior to Ref. [S6], in that the *slope* of the near-nodal gaps decrease with further underdoping, but the interpretation is different because laser ARPES reveals a gap at the nodal momentum in region **A**. In the simplest scenario, the gap measured below T_c in region **A** represents a sum of a *d*-wave superconducting gap ($\Delta_{SC}(\mathbf{k})$), a momentum-independent gap (Δ_{node}), and a momentum-dependent pseudogap ($\Delta_{PG}(\mathbf{k})$) of the form ${\Delta_A}^2={\Delta_{SC}(\mathbf{k})}^2+{\Delta_{node}}^2+{\Delta_{PG}(\mathbf{k})}^2$. Thus, v_A may indeed reflect *d*-wave superconductivity, but we argue that it decreases in region **A** because Δ_{node} increases, not because T_c decreases.

Fig. S5 shows the low-temperature energy scales plotted in Fig. 2(d) of the manuscript, scaled by T_c.

S.4. EVOLUTION FROM REGION B TO REGION A

Fig. S6 shows EDCs at k_F below and above T_c for samples in region **A** and **B**. We point out several features. First, the EDC at the nodal momentum in UD22 and UD34 exhibits a finite density of states at E_F. Some of this is intrinsic to ARPES experiments, arising from scattered electron which have lost their momentum information. The remainder may reflect a spatially and time varying phenomenon [S9], of which ARPES sees an average because of the large spot size and the time duration of data acquisition. Second, EDC widths at a given momentum show a smooth evolution from the most underdoped portion of region **B** into region **A**, indicating that samples in region **A** are not substantially more disordered than those in the underdoped part of region **B**. We point out similar behavior in CCOC where low-energy peaks are observed in gapped spectra for p=0.10 [S10].

EDCs at the antinode (Fig. S7) exhibit a change going from region **A** to region **B** at 10K. While the latter shows a remnant of a quasiparticle peak, reflecting a gradual suppression of this feature with underdoping (see Fig. S4(c)), the former exhibits featureless antinodal spectra. It is intriguing that antinodal quasiparticles are lost at the onset of region **A**. We cannot dismiss the possibility that this is a matrix element or disorder effect, but it is also possible that this loss is intrinsic, perhaps arising from a change in FS topology.

Fig. S8 compares UD34 (region **A**) and UD40 (region **B**) gaps at similar temperatures above T_c. While there is a small change in doping and T_c between the two samples, the gap functions above T_c are qualitatively different, with the former exhibiting a FS which is gapped at every momentum and the latter exhibiting characteristic pseudogap phenomenology with a Fermi arc. At intermediate momenta, gaps are comparable. This provides additional hints that the fully gapped FS in region **A** may be distinct from the pseudogap, with the pseudogap likely also persisting, though neutron scattering indicates that it may be weakened [S9].

S.5. FLUCTUATING SUPERCONDUCTIVITY

Evidence of superconducting fluctuations above T_c has been reported by a number of techniques, some reporting a very large onset temperature [S11, S12] and other yielding an onset close to T_c [S13, S14]. In Fig. 4(c) of the manuscript, we see a single spectral feature

above T_c whose phenomenology appears more consistent with the pseudogap, so we argue that while other experimental techniques can directly observe superconducting fluctuations above T_c, these features provide only a minority contribution to the spectral intensity seen by ARPES. The first indicator of this is the disappearance of upper Bogoliubov peaks above T_c, as shown in Fig. S9. A superconducting gap of magnitude Δ_{SC} opens symmetrically at k_F, and an EDC at k_F would have peaks at both ω=+Δ_{SC} and ω=−Δ_{SC} in the absence of a Fermi-Dirac cutoff. At higher temperature, there is a small thermal population of states above E_F, and the enhanced photon flux of laser ARPES allows us to collect data with sufficient statistics to discern these upper Bogoliubov peaks. The presence of the upper Bogoliubov peak is the clearest signature of superconductivity seen by ARPES in the cuprates, because much of the FS remains gapped above T_c (the pseudogap) so a gap by itself does not signal superconductivity. The upper Bogoliubov peak is less pronounced in more underdoped samples, because the T_c is lower, and the quasiparticle intensity tends to decrease with underdoping. EDCs at k_F are shown below and above T_c in Fig. S9 for four samples, and the peak/shoulder feature attributed to the upper Bogoliubov quasiparticle is marked by an arrow and shown to be absent above T_c. A finer sampling of temperatures for OD80 and UD92 (Fig. S9(e)-(f)) further illustrates the difference between superconducting spectra and non-superconducting spectra. Notably, these data appear outside of the arc region of the pseudogap phase, defined as momenta where symmetrized EDCs imply zero gap, so if an upper Bogoliubov peak is present above T_c, we should be able to observe it at those momenta. The second indicator that the gaps in Fig. 4(c) of the manuscript are of primarily pseudogap character is that they follow the well-established doping dependence of T* rather than the doping-independence of the superconducting gap in region **B**.

S.6. MEASURING T*

In Fig. 4(f) of the manuscript we show T* from ARPES, STS, and SIS tunneling experiments together, because these are comparable techniques where T* is determined by a suppression of antinodal density of states at E_F. If T* is sufficiently low to be accessible by ARPES, we use a standard definition [S15, S16], defining T* as the temperature when symmetrized antinodal EDCs at k_F exhibit a single peak at E_F, as shown in Fig. S10 (a). For more underdoped samples, T* is not reliably accessible by ARPES, because oxygen can

become mobile above T≈200K changing the doping near the surface during the course of an experiment. In those cases, T* is determined by extrapolating parameters measured in the pseudogap state at lower temperature, such as the spectral loss function [S16] or the fitted gap [S2], as shown in Fig. S10(b)-(d).

T* from other experimental techniques (in-plane resistivity, NMR, neutron scattering) are shown in Fig. S11 [S17–S19]. Neutron scattering data is shown for YBCO in Fig. S11, because data on Bi-2212 is currently not published. Though a number of experiments support a critical point of the pseudogap at p=0.19 [S20, S21], there are data from a number of experiments (transport, NMR, ARPES, tunneling) indicating a pseudogap persisting above T_c for p>0.19, as seen in Fig. S11; this is reconciled in the manuscript via evidence of phase competition between superconductivity and the pseudogap. Fig. S11 also plots data from experiments which directly observe a pronounced change in ground state superconducting properties at p=0.19, consistent with the critical point of the pseudogap: superfluid density [S20, S21], superconducting peak ratio [S5], and Cu-site doping required to destroy superconductivity[S21]. As discussed in the main text, a number of experiments on YBCO report an emergent phase at the underdoped edge of the superconducting dome, perhaps related to phase region **A** observed in Bi-2212. For comparison to ARPES data only zero magnetic field or low magnetic field results are shown in Fig. S11 [S9, S22], though we note that high field experiments yield similar critical dopings [S23, S24].

[S1] J. L. Tallon, C. Bernhard, H. Shaked, R. L. Hitterman, and J. D. Jorgensen (1995) Generic superconducting phase behavior in high-T_c cuprates: T_c variation with hole concentration in $YBa_2Cu_3O_{7-\delta}$. *Phys. Rev. B* 51:12911-12914.

[S2] M. R. Norman, M. Randeria, H. Ding, and J. C. Campuzano (1998) Phenomenology of the low-energy spectral function in high-T_c superconductors. *Phys. Rev. B* 57:R11093-R11096.

[S3] I. M. Vishik, et al. (2009) A momentum-dependent perspective on quasiparticle interference in $Bi_2Sr_2CaCu_2O_{8+\delta}$. *Nat. Phys.* 5:718-721.

[S4] I. M. Vishik, et al. (2010) ARPES studies of cuprate Fermiology: superconductivity, pseudogap and quasiparticle dynamics. *New Journal of Physics* 12:105008.

[S5] D. L. Feng et al. (2000) Signature of Superfluid Density in the Single-Particle Excitation

Spectrum of $Bi_2Sr_2CaCu_2O_{8+\delta}$. *Science* 289:277-281.

[S6] K. Tanaka, et al. (2006) Distinct Fermi-Momentum-Dependent Energy Gaps in Deeply Underdoped Bi2212. *Science* 314:1910-1913.

[S7] M. J. Lawler, et al. (2010) Intra-unit-cell electronic nematicity of the high-Tc copper-oxide pseudogap states. *Nature* 466:347-351.

[S8] R.-H. He, et al. (2011) From a single-band metal to a high-temperature superconductor via two thermal phase transitions. *Science* 331:1579-1583.

[S9] D. Haug, et al. (2010) Neutron scattering study of the magnetic phase diagram of underdoped $YBa_2Cu_3O_{6+x}$. *New Journal of Physics* 12:105006.

[S10] K. M. Shen, et al. (2004) Fully gapped single-particle excitations in lightly doped cuprates. *Phys. Rev. B.* 69:054503.

[S11] Y. Wang, L. Li, and N. P. Ong (2006) Nernst effect in high-T_c superconductors. *Phys. Rev. B* 73:024510.

[S12] L. Li et al. (2010) Diamagnetism and Cooper pairing above T_c in cuprates. *Phys. Rev. B* 81:054510.

[S13] J. Orenstein, J. Corson, S. Oh, and J. Eckstein (2006) Superconducting fluctuations in $Bi_2Sr_2Ca_{1-x}Dy_xCu_2O_{8+\delta}$ as seen by terahertz spectroscopy. *Annalen der Physik* 15:1521-3889.

[S14] M. S. Grbić et al. (2009) Microwave measurements of the in-plane and c-axis conductivity in $HgBa_2CuO_{4+\delta}$: Discriminating between superconducting fluctuations and pseudogap effects. *Phys. Rev. B* 80:094511.

[S15] T. Kondo, et al. (2011) Disentangling Cooper-pair formation above the transition temperature from the pseudogap state in the cuprates. *Nat. Phys.* 7:21-25.

[S16] A. Kanigel, et al. (2006) Evolution of the pseudogap from Fermi arcs to the nodal liquid. *Nat. Phys.* 2:447-451.

[S17] M. Oda et al. (1997) Strong pairing interactions in the underdoped region of $Bi_2Sr_2CaCu_2O_{8+\delta}$. *Physica C: Superconductivity* 281:135-142.

[S18] K. Ishida et al. (1998) Pseudogap behavior in single-crystal $Bi_2Sr_2CaCu_2O_{8+\delta}$ probed by Cu NMR. *Phys. Rev. B* 58:R5960-R5963.

[S19] B. Fauqué et al. (2006) Magnetic Order in the Pseudogap Phase of High-T_c Superconductors. *Phys. Rev. Lett.* 96:197001.

[S20] W. Anukool, S. Barakat, C. Panagopoulos, and J. R. Cooper (2009) Effect of hole doping on the London penetration depth in $Bi_{2.15}Sr_{1.85}CaCu_2O_{8+\delta}$ and $Bi_{2.1}Sr_{1.9}Ca_{0.85}Y_{0.15}Cu_2O_{8+\delta}$. *Phys. Rev. B* 80:024516.

[S21] J. L. Tallon, J. W. Loram, J. R. Cooper, C. Panagopoulos, and C. Bernhard (2003) Superfluid density in cuprate high-T_c superconductors: A new paradigm. *Phys. Rev. B* 68:180501.

[S22] X. F. Sun, K. Segawa, and Y. Ando (2004) Metal-to-Insulator Crossover in $YBa_2Cu_3O_y$ Probed by Low-Temperature Quasiparticle Heat Transport. *Phys. Rev. Lett.* 93:107001.

[S23] S. E. Sebastian, et al. (2010) Metal-insulator quantum critical point beneath the high T_c superconducting dome. *Proc. Nat. Acad. Sci.* 107:6175-6197.

[S24] D. LeBoeuf, et al. (2011) Lifshitz critical point in the cuprate superconductor $YBa_2Cu_3O_y$ from high-field Hall effect measurements. *Phys. Rev. B* 83:054506.

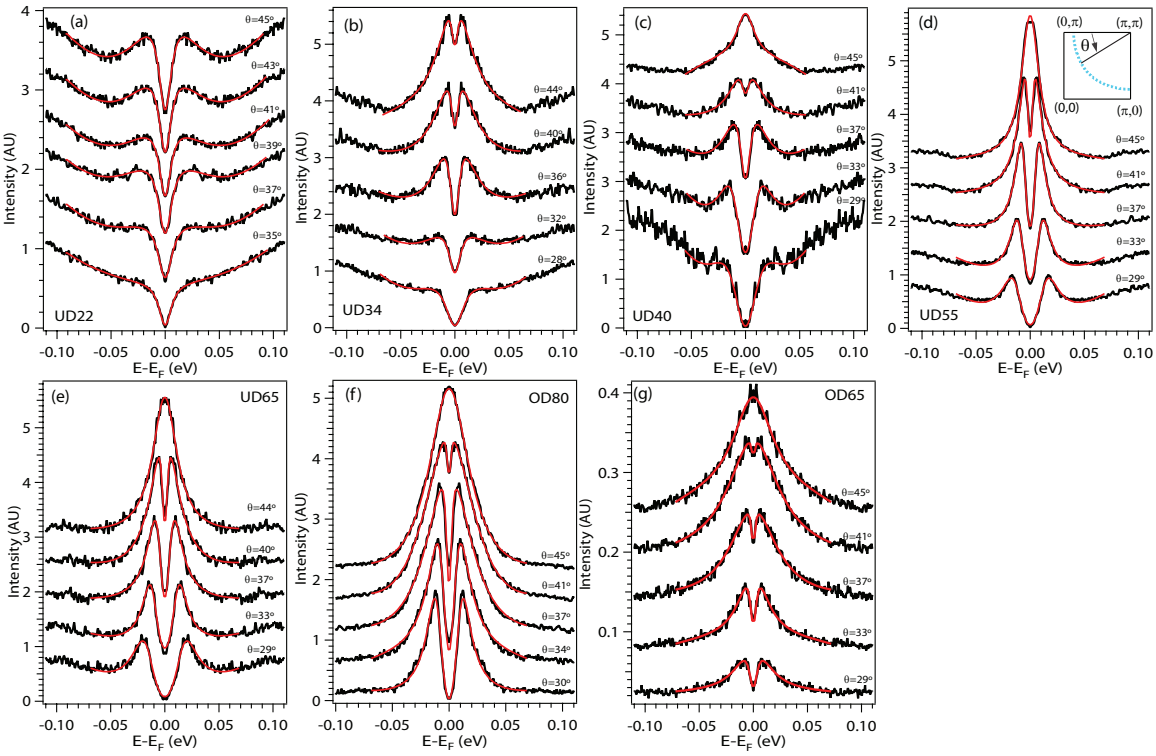

FIG. S1: Selected symmetrized EDCs at low temperatures with fits. All data taken with 7eV laser and cuts parallel to ΓY.

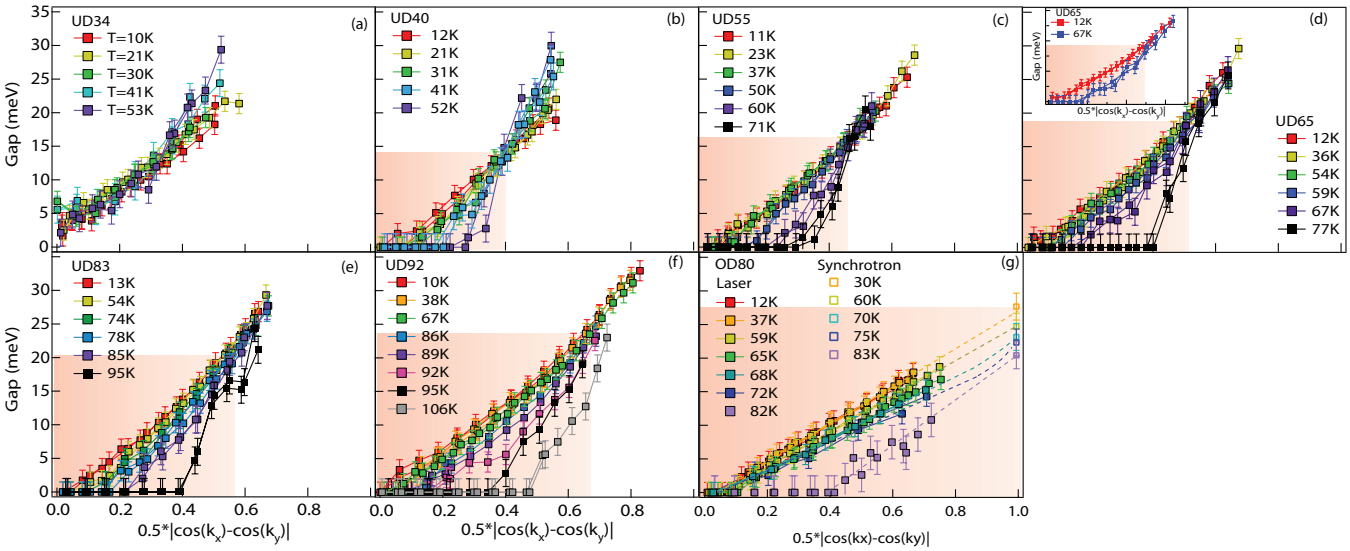

FIG. S2: Gaps from low temperature to T>T_c. Shaded region denotes momenta where gap T>T_c is smaller than low temperature gap, as explained in inset of (d).

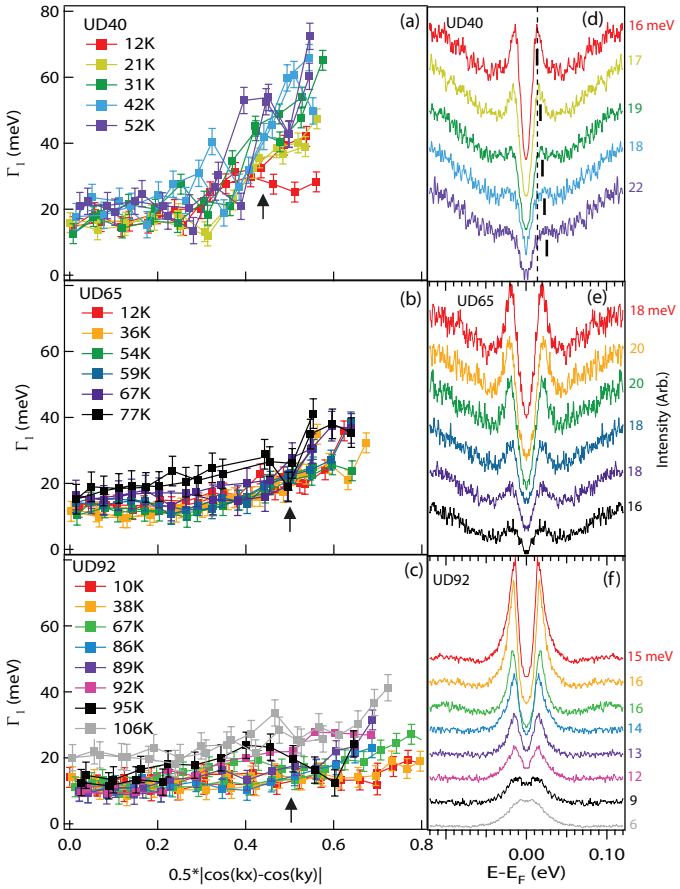

FIG. S3: Scattering rates and temperature dependence of EDCs. (a)-(c) Γ_1 [S2] from fitting for selected dopings. Error bars denote average 3σ confidence interval for each temperature. (d)-(f) Symmetrized EDCs at the cut position indicated by arrow in (a)-(c). Numbers to the right of panels indicate the gap value from fitting the EDC. In panel (d), dashed line denotes EDC peak position at lowest temperature, while short vertical lines denote peak positions at all temperatures.

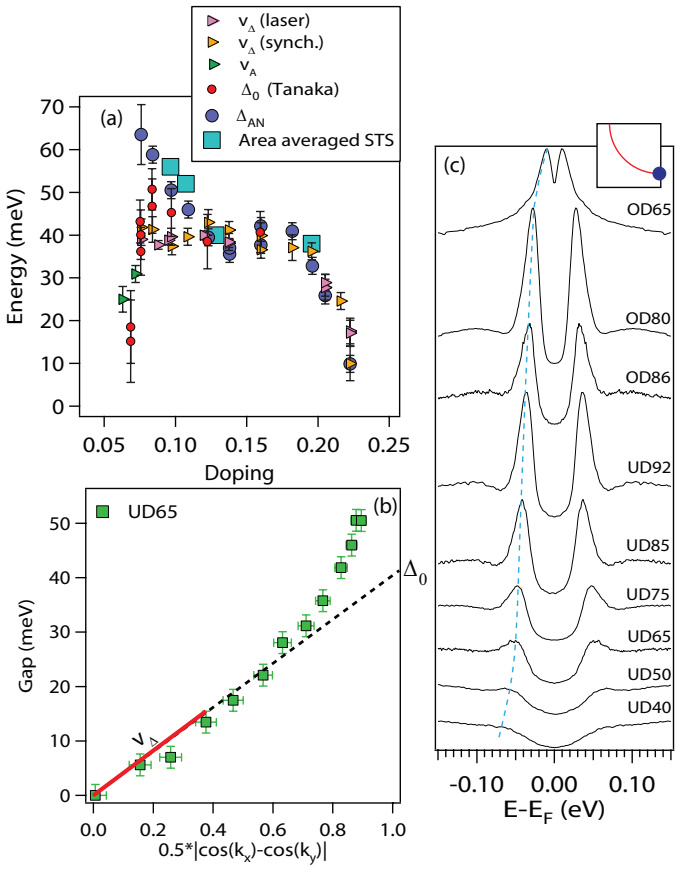

FIG. S4: Previously published data and antinodal gaps. (a) Comparison of near-nodal gap slope to previously published data (Tanaka, et al. Ref. [S6]). Data are consistent where they overlap except new results draw decisive conclusions about doping independence of v_Δ for $0.076 \leq p \leq 0.19$ and show that decrease of gap slope in deeply underdoped regime (v_A) happens in conjunction with the opening of a gap at the nodal momentum. Antinodal gaps (Δ_{AN}) are determined from fitting symmetrized EDCs. A gap function close to a simple d-wave form is realized when $\Delta_{AN} \approx v_\Delta$. Area-averaged STS energy gap from peak position at positive bias from curves in Ref. [S7]. (b) Definition of Δ_0 from Ref. [S6] and v_Δ from manuscript. (c) symmetrized EDCs at the antinode, in order of increasing doping from bottom to top. Dotted line is guide-to-the-eye for peak position.

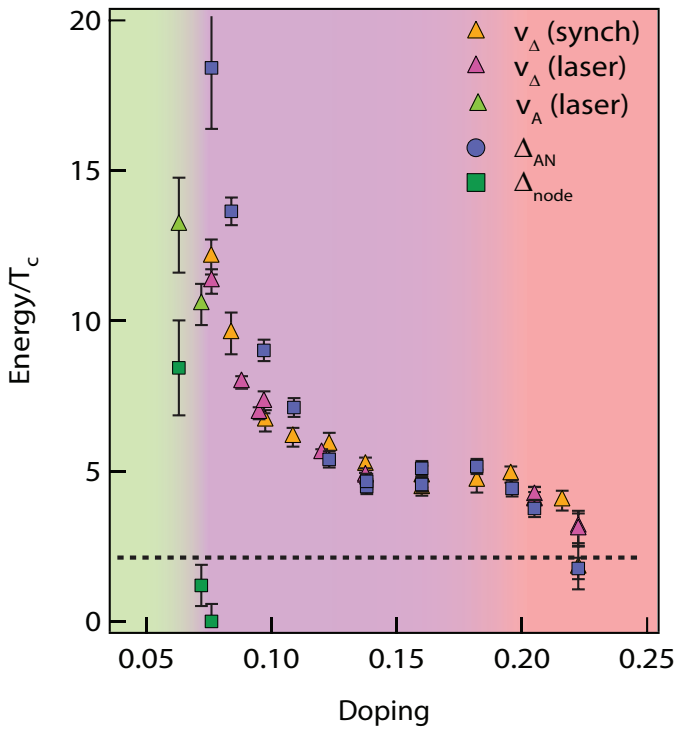

FIG. S5: Fig. 2(d) of the manuscript, including also Δ_{AN}, with energies scaled with T_c. Horizontal dashed line denotes the d-wave BCS ratio Δ/T_c=2.14

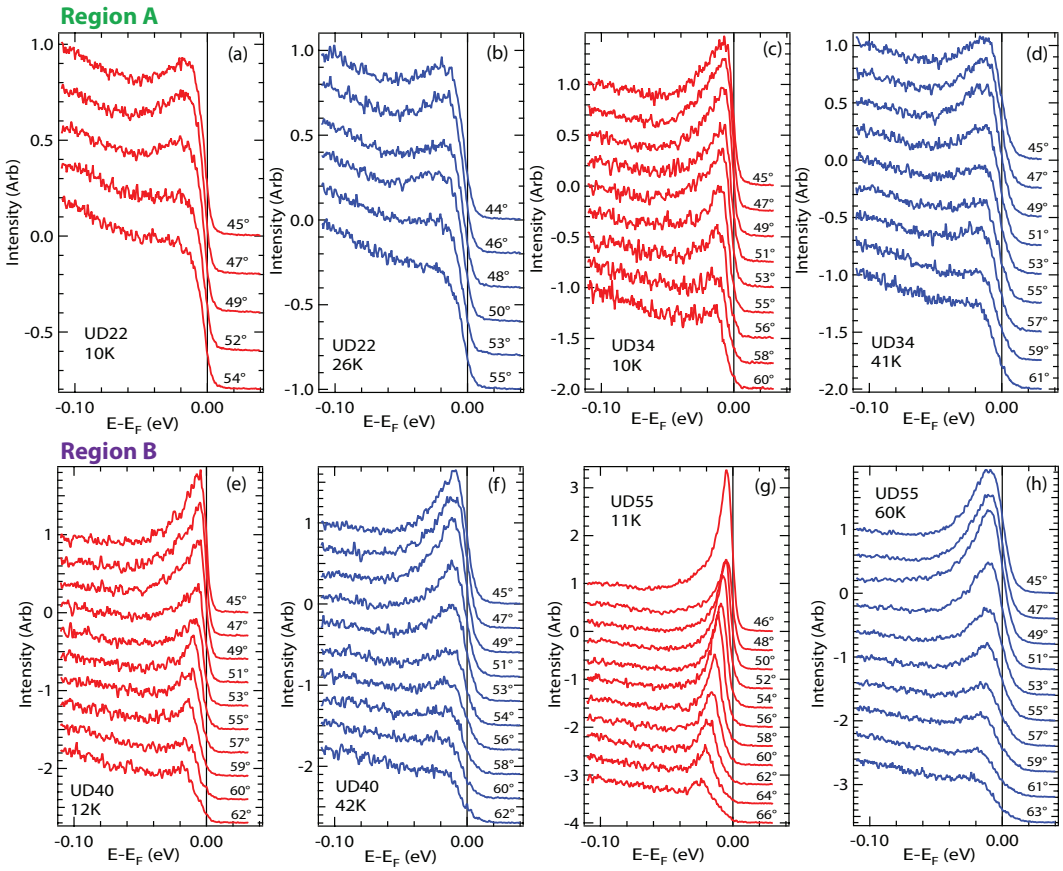

FIG. S6: Raw EDCs at k_f in region **A** and the most underdoped samples of region **B**, at low temperature (red) and above T_c (blue). EDCs are normalized to have equal intensity at 110meV. (a)-(d) Region **A**. Successive EDCs away from the node are shifted down by 0.2 (UD22) and 0.25 (UD34) in arbitrary units. (e)-(h) Region **B**. Successive EDCs away from the node are shifted down by 0.3 (UD40) and 0.4 (UD55) in arbitrary units. Sometimes different angles are sampled at different temperatures because of slight sample shifting. Angles farther away from the node are shown for larger dopings because the quasiparticle weight increases with doping making peaks in off-nodal spectra increasingly more pronounced.

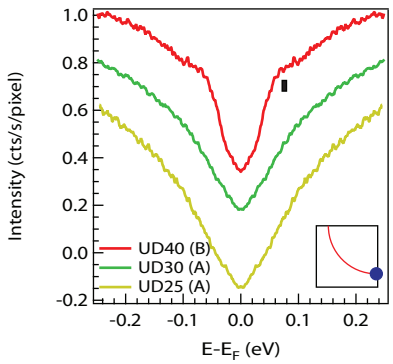

FIG. S7: Antinodal symmetrized EDCs for dopings in region **A** (UD30, UD25) and region **B** (UD40). Cuts taken parallel to ΓY at 10K with 19eV photons in the second Brillouin zone. While UD40 shows remnants of quasiparticles at antinode below T_c, antinodal spectra for region **A** samples are featureless.

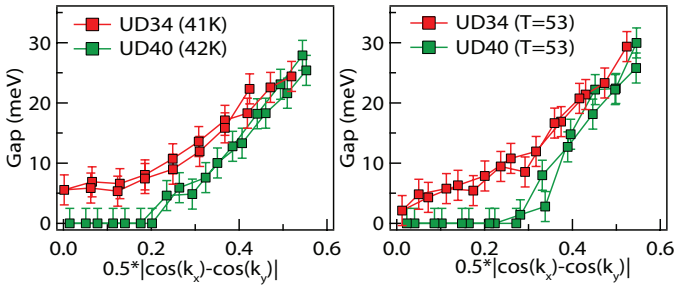

FIG. S8: Gaps above T_c for UD34 (p≈0.072, region **A**) and UD40 (p≈0.076, region **B**) at comparable temperatures.

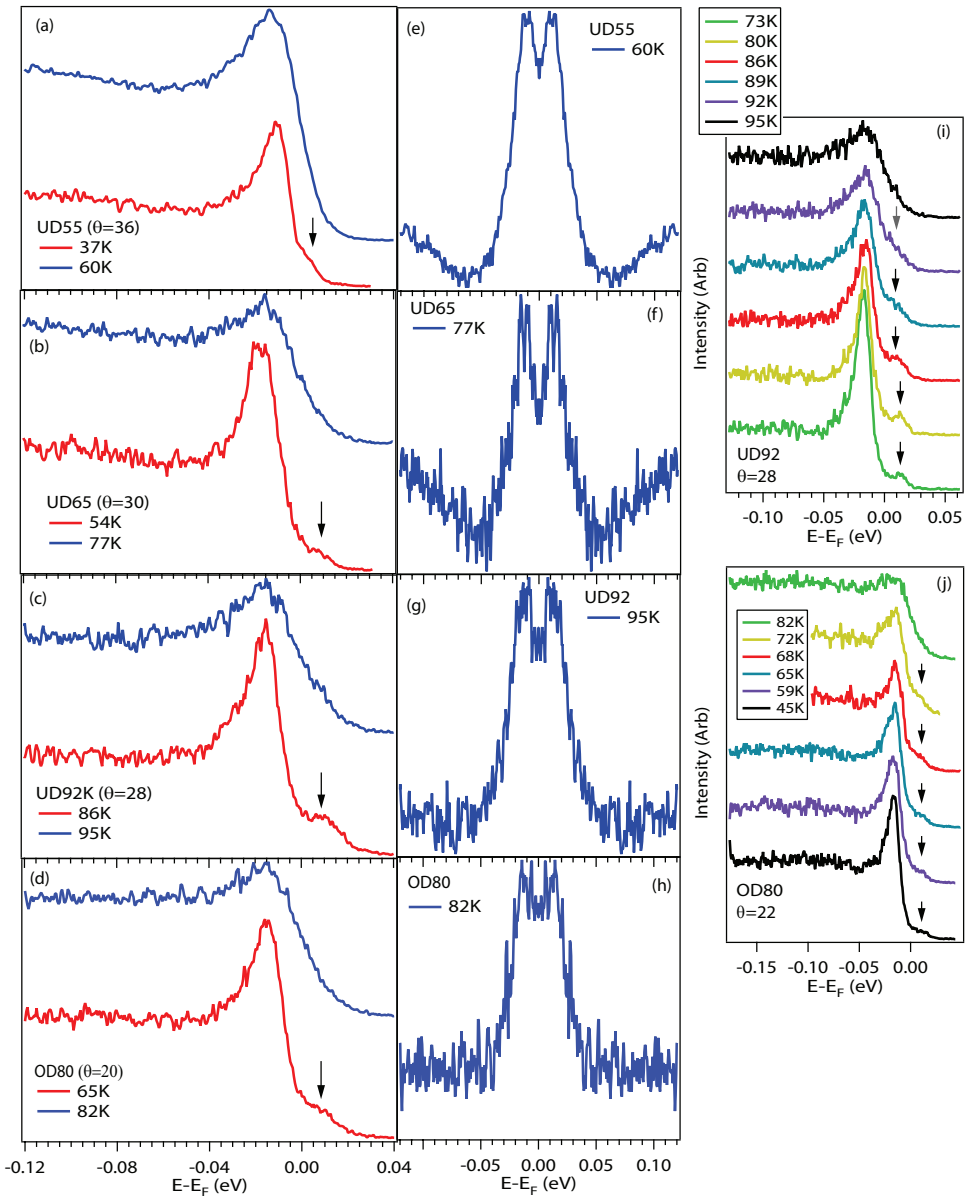

FIG. S9: Disappearance of upper Bogoliubov peak above T_c. EDCs at k_F, cut chosen to be in the gapped region for T slightly higher than T_c. (a)-(d) EDCs at k_F below (red) and above (blue) T_c for UD55, UD65, UD92, and OD80. Upper Bogoliubov peak is marked by arrow in $T<T_c$ data, but is not visible $T>T_c$. (e)-(h) Symmeterized EDCs for $T>T_c$, showing that spectra are still gapped at these momenta. (i)-(j) Temperature dependence of EDC at k_F for UD92 and OD80. Arrows mark upper Bogoliubov peaks, which disappear across T_c. FS angle θ defined in Fig. S1.

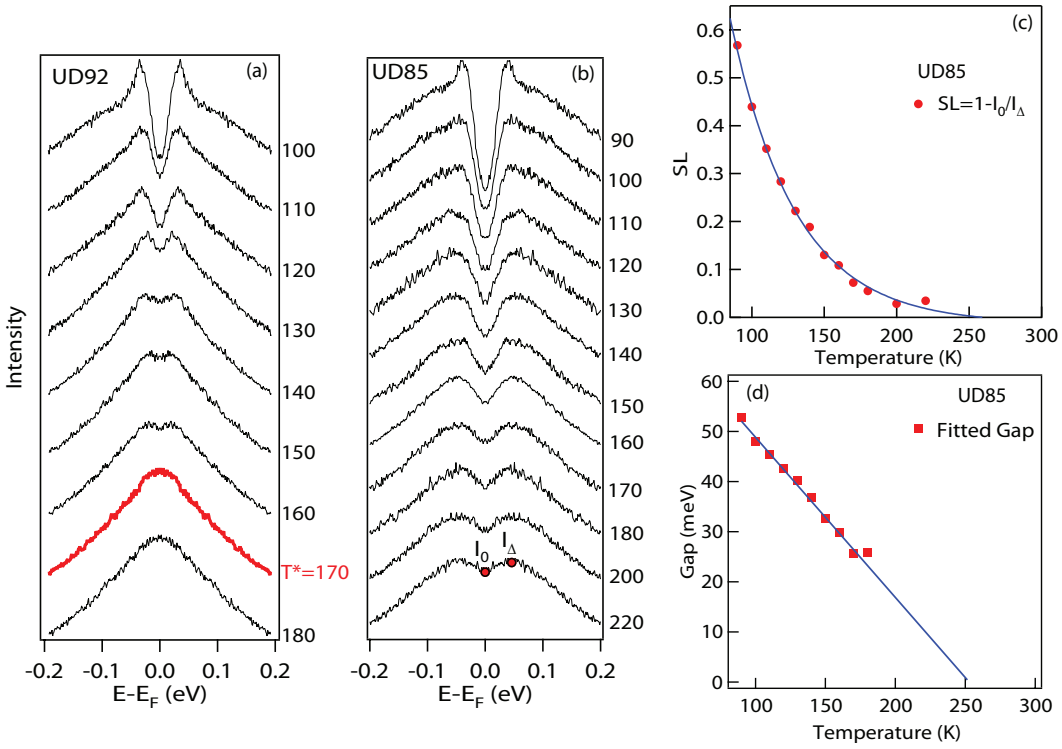

FIG. S10: Extracting T* from ARPES data. (a) UD92. Symmetrized EDCs at k_F T>T_c. T* highlighted in red, defined as temperature when symmetrized EDCs show a single peak at E_F. (b) UD85, symmetrized EDCs at k_F. (c)-(d) T* determined from extrapolating spectral loss function (SL)[S16] or fitted gap [S2]. Because antinodal spectra are considerably broader above T_c, an additional lifetime term is included in the fitting, as discussed in Ref. [S2].

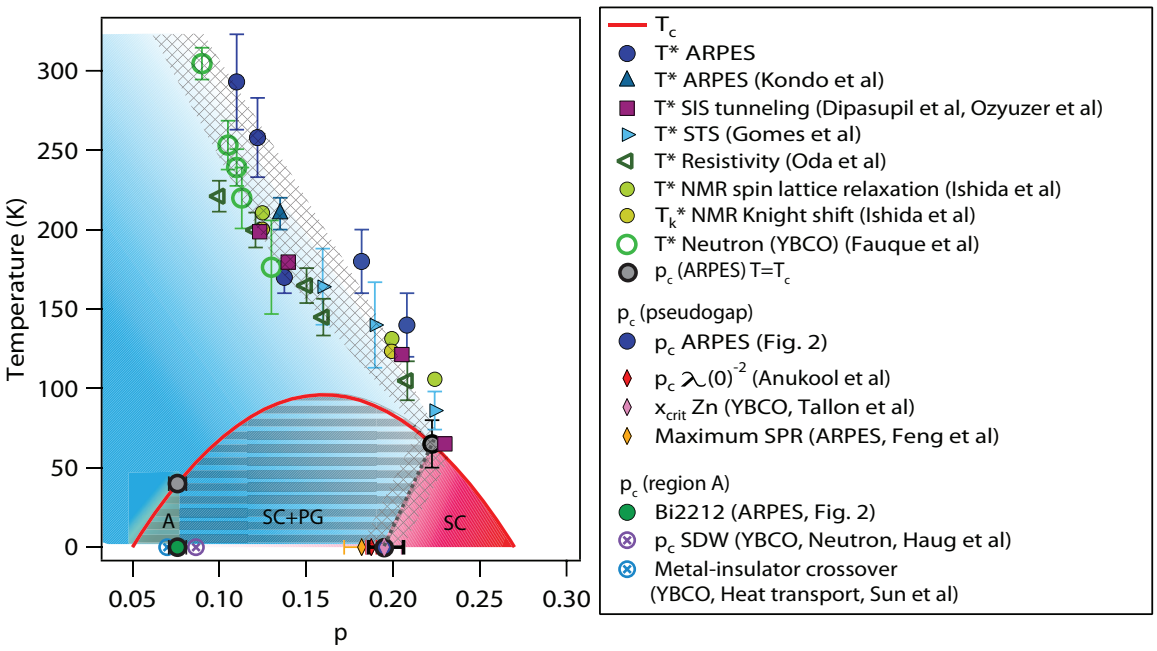

FIG. S11: Fig. 4 (f) from the manuscript and references therein, shown with T* data from other experiments: Resistivity [S17], NMR [S18], and Neutron scattering on YBCO [S19]. Low temperature measurements of pseudogap critical doping are indicated [S5, S20, S21]. Also shown are zero-field determinations of crossover ([S22]) or critical ([S9]) dopings measured in YBCO, together with the onset doping of region **A** from ARPES.